Robust statistical significance for Gravitational Wave inference

Alexandre S. Göttel*
School of Mathematical Sciences, University of Nottingham, Nottingham NG7 2RD, United Kingdom
(Dated: October 30, 2026)

The field of gravitational-wave data analysis heavily relies on Bayes factors to make statements about astrophysical effects in events detected by the LIGO-Virgo-KAGRA collaboration. This is true on an event level, for example when discussing the potential detection of precession or eccentricity, as well as on a population level. For the latter, perhaps the main limiting factor is the reliance on the output from event-level nested sampling analyses, which is known to introduce growing uncertainties and biases as the number of detections increases. In both cases, while Bayes factors are useful when comparing different models, because the underlying distribution of Bayes factors in noise is unknown, it is often not possible to use them to make quantifiable statistical statements. Their statistical meaning is also questionable in the at least 20% of GW events that contain transient noise artifacts. This paper shows that it is possible to use evidence networks, which can infer Bayes factors after learning the distinguishability between datasets, to solve all of the aforementioned problems. By being able to calculate up to 10^5 Bayes factors per second, we can construct background distributions of Bayes factors under different signal assumptions to estimate significance. We show that the high precision achieved allows us to scale the results from up to 10^4 events with no discernable bias on population-level quantities, while laying the foundations for a likelihood-free method that does not rely on the assumption of Gaussian and stationary noise.

arXiv:2610.39785v1 [astro-ph.IM] 29 Oct 2026

I. INTRODUCTION

Gravitational-wave data analysis has from before the first detection to today been dominated by Bayesian approaches. More specifically, the parameter estimation of all LIGO-Virgo-KAGRA (LVK) catalogues [1–4] were performed using a Bilby-implementation of the Dynesty Nested-Sampling algorithm [5, 6]. The primary design goal of nested sampling is to estimate the so-called *evidence* $\mathcal{Z}$, obtained by integrating the prior-weighted likelihood over the entire, typically high-dimensional, parameter space. It encodes all necessary information for model comparison, and is mostly used to calculate Bayes factors which, assuming equal prior odds, equals the posterior odds at which one hypothesis is preferred over another.

The calculation is very costly, uncertain, and in the case of all compact binary coalescence (CBC) parameter estimation by the LVK relies on the assumption that the detector noise is perfectly Gaussian and stationary. Both of these assumptions are known to be false, as for example at least 20% of GW detections contain transient noise artifacts [7], but deliver 'good-enough' results for most events.

This study applies a new method [8] that uses machine learning to directly estimate Bayes factor from data by exploiting underlying statistical differentiability. This amortized method can not only be used to reduce the time-to-delivery of astrophysical information to $\mathcal{O}(1\,\mathrm{s})$ (as opposed to days or weeks with nested sampling), but, most importantly, also does not require a formal definition of the likelihood or priors. Any working implementation can thus in principle be trivially extended to learn directly from any available data, including real (non-Gaussian, non-stationary) interferometer data. Contrary to nested sampling, this thus allows one to calculate meaningful Bayes factors on real detector noise. It could also for example be used for unmodelled glitches or waveform systematics, and can in theory be used directly on a population level - effectively obtaining astrophysical results while bypassing the entirety of a traditional sample-based catalogue's parameter estimation work.

This paper introduces the aforementioned method to gravitational wave data analysis for the first time, and applies it to the detection of general-relativistic precession in CBCs, both on an event- and population-level. Section II establishes the method in the context of GW precession measurements. Section III describes the training procedure and modifications specific to GW data analysis. Section IV compares our results with state-of-the-art approaches and introduces a method to obtain statistical significances, illustrated by a mock search for precession. It further applies the method to sample-free population inference, demonstrating accurate recovery of population variables for populations up to 10^4 events, where conventional hierarchical Bayesian approaches would be biased by large Monte-Carlo uncertainty [9, 10] and incur prohibitive costs.

II. BACKGROUND

A. Evidence networks

Evidence networks are simple binary classifiers that are trained to differentiate between two dataset. The idea is that with a clever choice in the loss function, one can calibrate the optimal network output, given observed data $x_{\mathcal{O}}$, to be a trivial transform of the Bayes factor $\mathcal{B}$ be-

* alexandre.goettel@nottingham.ac.uk

tween the two models. Because the output of such a network is just a single number, one essentially bypasses the high-dimensional calculations (and accompanying uncertainties and numerical instabilities) that are typically required, for example when using nested sampling. This is possible because the loss exploits the statistical properties of the Bayes factor as a discriminator in data-space directly, instead of trying to derive it through integration. The drawback is that such losses necessarily include exponential terms, which because of the behaviour of their gradients are notoriously difficult to handle with deep learning.

It is worth noting that in theory, the widely-used binary cross-entropy loss could also be used. After all, it outputs probabilities which can be converted to Bayes factors. However, in practice, since neural networks can typically only handle numbers of $\mathcal{O}(1)$ when back-propagating gradients over several layers, one can't expect them to be reliable in probability spaces where one model is strongly preferred over another. Additionally, standard classifier training generally struggles with the precision needed for meaningful model comparison, and often produces overconfident results [11]. While this is not necessarily a problem for pure classification tasks, it renders it practically impossible for such approaches to be accurate beyond an overly narrow range of Bayes factors in this context.

The work in this paper is based on [8], where methods were explored to counteract this problem. Specifically, we use the 'leaky' parity-odd power (l-POP) exponential loss function. It is defined as:

$$\mathcal{L}(f(x), m) = e^{(\frac{1}{2}-m)\mathcal{J}_\alpha(f(x))}, \tag{1}$$

where $m \in [0, 1]$ denotes the source of the data x, and $f(x)$ represents the output of the network applied to the data. The l-POP transform $\mathcal{J}_\alpha$ is defined as:

$$\mathcal{J}_\alpha(x) := x + x|x|^{\alpha-1}. \tag{2}$$

Though one could replace $\mathcal{J}_\alpha$ with any monotonic function and still obtain valid results, we find, in line with the original publication, that using it leads to more stable network training. The reason for using this exponential loss is, as outlined in [8], that an *optimal* network $f^*(x)$, trained to reach a global minimum on this loss, will output a simple transform of the Bayes factor $\mathcal{B}$ for observed data $x_\mathcal{O}$, with:

$$\log \mathcal{B} = \mathcal{J}_\alpha(f^*(x_\mathcal{O})). \tag{3}$$

B. General-relativistic Precession in GW data

In binary black hole (BBH) systems, precession stems from the misalignment between the orbital angular momentum and the total spin of the individual black holes. The effects of general-relativistic precession have long been studied, and its possible imprints on gravitational waves are generally well understood, at least in theory [12, 13].

Precession is of particular astrophysical interest, as its detection is a clear indication of the formation channel of the binary. Indeed, while many models of BBH formation exist, it is commonly accepted that the two main expected categories are binaries formed with a common envelope, and those formed in the presence of dynamical interactions in high-density environments [14]. The former implies friction that would force the component spins to align with the orbital angular momentum, while in the latter the spins are expected to be isotropic. A confident detection of precession, along with the properties of said system, would therefore inform us on the fraction of events from each formation channel, and greatly impact models on the role of clusters in the BBH population [15]. It would also help to understand pair-instability supernovæ which would in turn impact models of stellar evolution, notably given the sensitivity of the pair-instability mass gap to the $^{12}\mathrm{C}(\alpha,\gamma)^{16}\mathrm{O}$ reaction rate [16].

There is to date but a single GW event for which substantial evidence for precession has been claimed: GW200129 [17–19], and even in this case the results are disputed. In particular, while [19] find roughly 1:25 000 odds in favour of precession, [20] finds that the difference in the data between precessing and non-precessing hypotheses is lower than the statistical uncertainty resulting from methods used to remove known excess noise from the data. However, other studies using different methods of noise mitigation [21, 22] find compatible results with [19] (though neither quantifies the significance of a potential measurement of precession). In any case, it is noteworthy that the only event with such strong claims is also known to have excess noise in precisely the frequency range in which the evidence for precession originates [20].

Generally, the main obstacle behind the detection of precession is that its leading order effect on GW waveforms as measured from Earth vanishes when the BBH is face-on. Such BBH systems have a higher signal-to-noise ratio (SNR) and are therefore the most common type of detected systems. When factoring in knowledge from population studies, [18] finds that only about 1 in 50 events can be expected to have a *significance* imprint of precession. While the meaning of *significance* is somewhat up to interpretation since the data includes GW200129, even in optimistic scenarios the evidence for the presence of measurable precession is quoted to be less than 3σ when considering all events in GWTC-3 [17].

III. METHODS

A. Data

One limitation of Bayes Factors in general is that their calculation assumes that the models are well chosen. This applies here as well, since extreme Bayes Factors can arise

when one or both models fail to accurately represent the data [23]. It is thus worth mentioning here that this method is not intended to

As mentioned in Section II A, evidence networks are, in essence, classifiers trained to differentiate between two datasets (say, A and B), calibrated such as to output (up to a trivial transform) the Bayes factor between said datasets. Two such networks are trained in this paper. The first is trained to obtain the Bayes factor for precession. In this scenario I, data from model A is generated by simulating gravitational-wave strain using default isotropic-spin priors as used by the LIGO-Virgo-KAGRA collaboration [7]. Data from model B is identical, with the exception that component spins are forced to be aligned with their respective orbital angular momentum. While we use the IMRPhenomXPHM [24] approximant to generate both datasets, we further constrain the mass priors be compatible with the posteriors obtained for GW231123 [25], and to be compatible with NRSur7dq4 [26], to allow for these analyses to be re-used in future publications. More details on the priors can be seen in Table I.

A scenario II is also introduced, where both models use identical priors, but their data are generated using A: IMRPhenomXPHM [24] or B: IMRPhenomPv2 [27, 28] (which does not model multipoles beyond the 22 mode). This scenario was explicitly designed to generate data with low Bayes factors in order to simplify network training, and such that Bilby analyses using the scenario will finish in minutes. This will be useful in later sections of this paper where $\mathcal{O}(10^2)$ Bayes factors are computed with Bilby to validate the networks. Given the computational costs associated with nested sampling, this would not be feasible at this scale for scenario I.

Scenario	**I**	**I**	**II**
Parameter	**Model A Precessing**	**Model B Aligned-spin**	**Model A/B Fast**
chirp_mass	85–195	–	80–120
mass_ratio	1/6–1	–	1/8–1
total_mass	60–400	–	N/A
D_L	10^3–10^4	–	4000
geocent_time	default	–	–
phase	default	–	–
dec	default	–	0.3
ra	default	–	4.4
θ_{JN}	default	–	0.75
ψ	default	–	1.7
a_1	default	–	0
a_2	default	–	0
tilt_1	default	0	0
tilt_2	default	0	0
ϕ_{jl}	default	0	0
ϕ_{12}	default	0	0

TABLE I. Priors used to generate gravitational wave data for the different scenarios. The defaults refer to uninformative priors as used in LIGO-Virgo-KAGRA catalogues [4].

Data from all models are generated in the frequency domain from 20 Hz to 224 Hz, a resolution of 0.25 Hz, and a reference frequency of 10 Hz. Coloured Gaussian noise is added using a PSD generated with the "aLIGO" configuration of pygwinc [29] and in the Hanford detector [1] only.

B. Training

Neural network training famously works best when the weights and biases are of $\mathcal{O}(1)$. In the field of gravitational-wave data analysis, it is not rare to see $\log \mathcal{B} \approx \mathcal{O}(10^2)$, for example when calculating the odds of there being a gravitational wave in noisy data. However, one can quickly see that even for $\log \mathcal{B} = \pm 20$, loss (see Equation (1)) values will reach $\mathcal{O}(10^{\pm 8})$. This is unavoidable since exponential terms are necessarily part of a loss that is used to output log Bayes factors, and represents a huge challenge for backward propagation even over a few layers. This section discusses the methods used to make training possible and reliable in this difficult loss landscape.

The first and most obvious step to avoid gradient explosion is to make sure that the training data does not contain examples with a corresponding $\log \mathcal{B}$ outside of a roughly ± 50 range where float precision will start failing in the exponential terms. For problems leading to such extreme values of $\log \mathcal{B}$, it is anyway questionable whether it is sensible to compare the two models in the first place.

A series of steps can then used to directly affect gradient updates: 1. gradient clipping, meaning that after backpropagation all gradients above a certain threshold are capped at the threshold value before the optimisation step occurs 2. batch normalisation, where layer inputs are normalised in each batch during training and an average normalisation is applied during validation 3. initialising the biases of the final layer to zero, and the weights in a $\pm 10^{-3}$ range. This dampens gradients in the initial training steps where the learning rate is usually highest, preventing erratic trajectories following a bad initialisation from leading to an unrecoverable state (which can easily occur in areas where the loss saturates because of the exponential term). Finally, 4. using an optimiser with a global approach to weight updates, like stochastic gradient descent, instead of one using adaptive methods. This was empirically found to be absolutely necessary to avoid overfitting as well as gradient explosion.

The combination of all the steps above lead to training that could individually reliably converge but would fail to be consistent in their answer over multiple training, with final loss values shy of a global minimum. This would typically mean networks that give trivial answers outside of a relatively small $\log \mathcal{B}$ range around zero. This is easily understood in the context of both scenarios studied in this paper, since the majority of data points have low evidence and the optimiser has much more

to loose than to gain when moving into the tails of the distributions. This problem was solved by using a so-called GrowNet [30] approach. This consists of training a secondary network, identical to the original one with the exception that, next to the training data, it also has access to the output of the penultimate layer of the pre-trained network. Simply put, the idea is that the first network training will find a solution that will satisfy the "bulk" of the data, while the second iteration will be able to focus on applying corrections to it, thereby reaching the next leading order. This was found to greatly stabilise the output of the networks and reliably make them reach lower loss values (see Section III C).

It is worth mentioning that besides the exponential gradients, another reason for difficulties during training is that, in order for the networks to actually output Bayes factors instead of only acting as classifiers, the training data must be generated by exactly following the prior. One can thus not generally apply transforms that affect data space to make training easier unless they can be shown to be orthogonal to the differentiability of the datasets. Similarly, any embedding must be lossless *w.r.t.* the prior because if an area of parameter space is affected more strongly by compression than an other, one is effectively changing the prior. This would change the evidence and thus the Bayes factors. This also means that the training data must be large enough such that even areas of low prior probability are *seen* by enough training iterations.

Training in this paper is done by concatenating amplitudes and complex angles of $4 \cdot 10^6$ frequency-domain GW waveforms, and using a relatively simple architecture (see Table II), owing to the simple binary-classifier nature of the networks. The training used a learning rate of $6 \cdot 10^{-4}$, momentum of 0.94, weight decay of $4 \cdot 10^{-4}$, a gradient clip of 0.16, and a batch size of 500.

Layer	Contents
Input Layer	512 neurons
(x4) ResNet Block	3 layers, 128 neurons each
Output Layer	1 neuron

TABLE II. Architecture of the evidence networks used in this paper. All activation functions are LEAKY RECTIFIED LINEAR UNIT [31] except the last one which uses Equation (2).

C. Validation

As mentioned in Section II A, an optimally trained evidence network will output a trivial transform of Bayes factors. However, there is never a guarantee that a network has indeed reached a global minimum, even when its validation loss has reached a plateau. It is therefore important to use other means of validation. This section outlines *blind coverage testing*, adapted from [8], and discusses further training and network consistency checks.

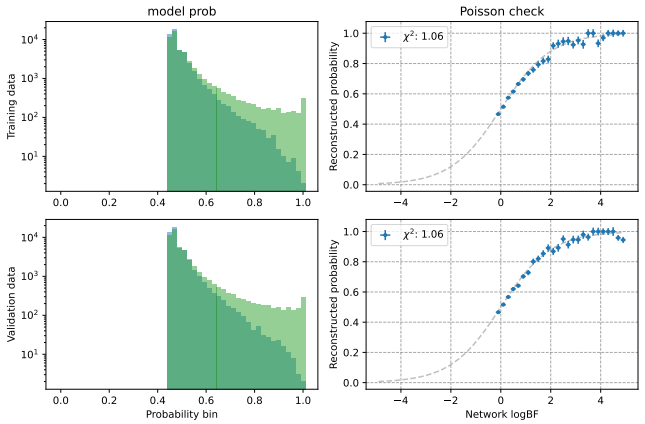


FIG. 1. Blind coverage and χ^2 tests using 10^5 waveforms. *upper*: using training data *lower*: using validation data *left*: histogram of $p(M_A|x)$ values (see Equation (4)) where green and blue denote data from models A and B, respectively. Because model B is a subset of model A, one would not expect strong evidence for model B, hence the lack of values below about 0.5 *right*: the data points are the ratio between the numbers in each histogram bin with Poisson-derived uncertainties, and the dashed curve shows Equation (4). As one can see, the output conforms to expectation.

Blind coverage testing makes use of the statistical properties of the Bayes factor, namely that for equal prior odds it is equal to the odds ratio. It follows that:

$$p(M_A|x) = \frac{\mathcal{B}}{1+\mathcal{B}}, \tag{4}$$

where $p(M_A|x)$ is the probability of model A being true given the data x. Using validation data (i.e. data that a trained network has not *seen*), one can thus simply use this equation to calculate $p(M_A|x)$ for every data point to construct a histogram. When using the same number of data points from each model, one would expect that in each bin, the relative number of entries from each model corresponds to the predicted probability. By assuming the numbers each bin to be independent and Poisson distributed, one can perform a χ^2 test where the number of degrees of freedom is the number of bins. The result of this test for Scenario I can be seen in Figure 1.
While *necessary*, this test is not *sufficient* to prove that the networks have correctly converged. A further validation test thus compares the output of separate networks trained on the same input data. Should the training procedure be valid, one would expect the networks to converge to the same result. For this test, N networks are separately trained with the same pre-determined procedure and on the same training data. The standard deviation of the outputs is then calculated for every waveform in the validation data and neighbouring values (in $\log \mathcal{B}$) are then averaged to give a representative impression of the network consistency. Figure 2 shows the output of this test, again for Scenario I. One can see that the GrowNet approach (see Section III B) has

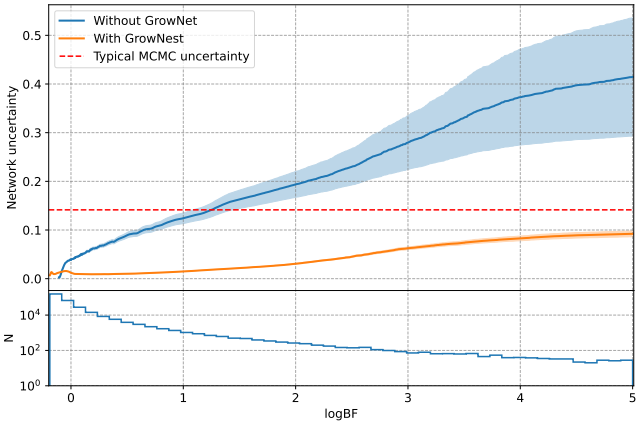


FIG. 2. With and without GrowNet (see Section III B), the standard deviation between five trained evidence networks as a function of the Bayes factor. The band shows the uncertainty on the estimated sample standard deviation, and the red line at $\sqrt{2}/10$ shows a typical uncertainty on log Bayes factors obtained from nested sampling.

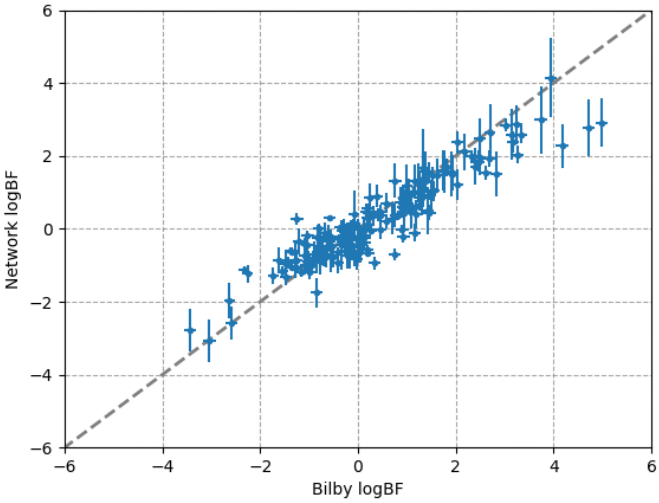


FIG. 3. 200 log Bayes factors obtained with the evidence networks against log Bayes factors obtained with Bilby. The y errors are estimated by training 5 networks and calculating the standard deviation between their outputs. As one can see, the data mostly fits the dashed $x = y$ line.

a significant impact on the training consistency. In this example, while uncertainties predictably increase in areas where there is less training data, it is nevertheless clear that the networks are consistent over the entire considered range of Bayes factors, and that their precision outperforms nested-sampling approaches by up to an order of magnitude. It is worth mentioning that this test can also be used to estimate the uncertainty of individual networks, which is not available when training a single network.

Another straightforward test is to compare the output from the networks to established methods. This is expensive to do using problems like Scenario I, which is why Scenario II was introduced. This is a simple four-parameter inference in which the free parameters are chirp mass, mass ratio, geocentric time, and phase. Bayes factors from Bilby we obtained using waveforms from the validation data. Since one inference takes about 5 min using Bilby (10 min per Bayes factor), it would not be feasible to estimate 10^5 Bayes factors as was done in Figure 1. Instead, 200 Bayes factors were calculated with Bilby and compared to the average output of five evidence networks, see Figure 3, with uncertainties estimated from their sample standard deviation as mentioned above. As one can see, the results mostly agree, with a few exceptions where the deviation is significant given the low uncertainty between the network results, though it never deviates by more than 2. Repeated training with different settings showed that these differences are persistent *i.e.* that the output from the networks is very consistent. Another possibility is that the uncertainty from Bilby (when run with a default dlogz=0.1) is underestimated. It is important to note that nested sampling also cannot generally obtain valid evidence values, as it can always miss sharply peaked modes in the likelihood structure during the integration process. Figure 4 puts this hypothesis to the test, and one can indeed see that under a blind coverage test (see above), the networks outperform Bilby. This is consistent with [8] where it was found that evidence networks outperform likelihood-based approaches, at least on a toy problem.

Finally, a fundamental limitation of this approach is tied to Bayes Factors in general: their calculation assumes that the models are well chosen. This applies here as well, since extreme Bayes Factors can arise when one or both models fail to accurately represent the data [23]. It is thus worth mentioning here that any results from this method can only be trusted if care was taken to demonstrate that the observed data lies well within the training data distribution.

IV. DISCUSSION

A. Precessing SNR

The so-called *precessing SNR* (ρ_p) was proposed in [32, 33] to help make statements about the detectability of precession. The idea is, having found that over the majority of the BBH parameter space the first two terms of the leading order precessing harmonics are the most significant, and given that both must be measurable for precession to be detected, one can simply define the minimum SNR of those harmonics as that with which precession can be detected. The main benefit of this approach is that the null hypothesis leads to a clearly defined back-

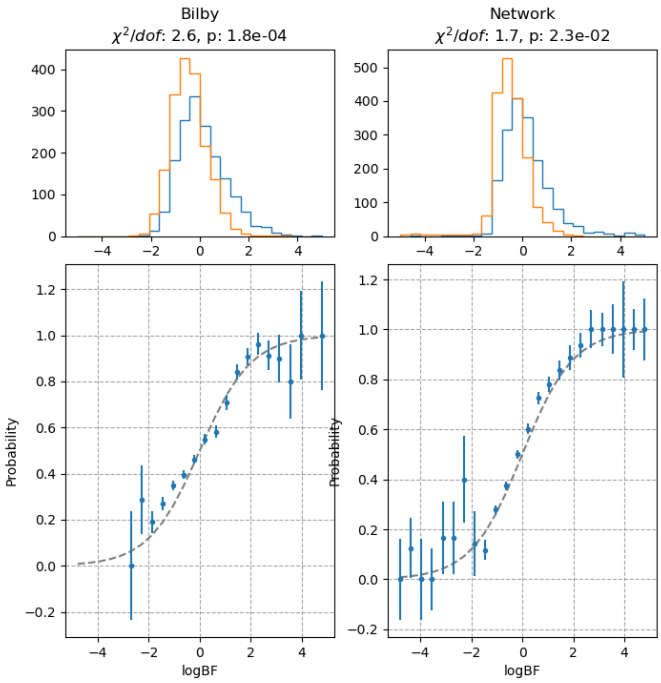


FIG. 4. Blind coverage test using 200 waveforms *left*: BILBY and *right*: evidence networks. The histograms on top show the logBF distribution from the two models of scenario II, and the curves show the χ^2 test (see Section III C). One can clearly see that although both approaches give similar overall results, that the networks outperform Bilby on this problem.

ground distribution. Indeed, from noise only one would expect ρ_p to follow a χ distribution with $k = 2$ degrees of freedom. Thus, by using the samples from a nested sampling run in a precessing parameter space, one can obtain a significance against the hypothesis that the observed precessing SNR is due to noise. By additionally using samples from a nested sampling run following an aligned-spin hypothesis, one can further inform the prior on ρ_p to obtain a more accurate significance [13].

As argued in [13, 32], while this approximation is very useful (and has been adopted by the LIGO-Virgo-KAGRA collaboration to make claims about precession [25, 34]), it is only valid when the precession angle is small. Therefore, while the assumptions are valid for a large majority of observed gravitational waves, they will reach their limits precisely when the potential for a significant measurement is highest. This is true for areas of parameter space with high mass ratios, maximal χ_p values, or when $\chi_{\rm eff} \leq -0.4$ (though at least two of the three above are required).

This lack of validity over parts of the parameter space is in theory addressed by the use of evidence networks, though a large dedicated explorative study to verify this is outside of the scope of this paper. In the context of this paper, the main limitations of ρ_p are rather that it relies on the assumption of Gaussian and stationary noise, and requires a preliminary nested sampling run

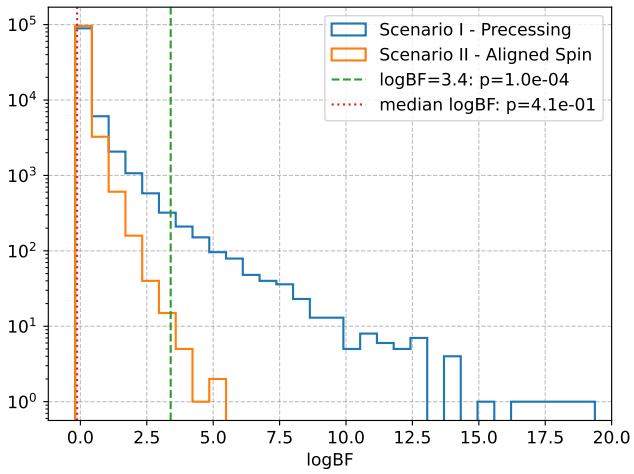


FIG. 5. Distribution of Bayes factors calculated with data from scenarios I and II. As expected given the prior, most values are close to zero but the distributions can be clearly distinguished by their tails.

(or two if informed priors are used).

B. Background Bayes factor distribution

While it is standard practice to calculate Bayes factors to make statements about precession (or other potential physics) in GW data [19, 25, 35–37], it has in practice not been possible to use them to claim the detection of precession in a real event. The main reason is that the background distribution of Bayes factors in interferometer noise is unknown, making it impossible to evaluate the significance of a result. For example, [25] finds Bayes factors upwards of 10^3 in favour of precession in GW231123 but is unable to claim a measurement. In the case of GW200129 [17] a much more modest Bayes factor of about 30 is accompanied by a much more significant claim of a measurement by using the *precessing SNR* [19]. This is also supported by [18] in the context of GWTC-3.0 [17] data, where p-values obtained using the aforementioned *precessing SNR* were compared to their expected distribution in noise for 69 events.

This paper solves this problem, as the trained networks are light-weight and can be used to calculate up to 10^5 Bayes factors per second (this includes reading data from disc and transferring the Bayes factors back to the CPU), making it trivial to construct background distributions. Figure 5 shows the distribution of Bayes factors for aligned-spin and precessing data. As expected, the precessing curve has a longer tail. In order to obtain a significance against the aligned-spin hypothesis, one can simply integrate the aligned-spin histogram up to the observed Bayes factor. In this example, a log Bayes Factor of 3.4 would correspond to a p-value of $\approx 10^-4$.

The ability to calculate a significance (e.g. for preces-

sion) from a Bayes factor alone is a very useful result on its own. However, the more important potential result, though it is beyond the scope of this publication, is the method's ability to perform the calculation with no assumption of Gaussian or stationary noise. When obtaining a Bayes Factor from nested sampling, one can sometimes obtain extreme values which are due to one or both of the models railing against a prior bound. Because in such cases the data cannot be accurately represented by the models, these Bayes Factors are rendered pointless [23]. The same is true of this method, which operates on the assumption that the models are well-chosen.

C. Scalable population inference with no samples

The most straightforward way to apply the methods presented in this paper to make statements on a population scale is to modify the way that the training data is generated. Using a selection function, one can build individual populations to give as input to the networks, similarly to what was done in [38, 39]. The main difference in this case is that evidence networks don't need to reconstruct multi-dimensional surface distributions in order help make astrophysical statements, and are as such much smaller and faster to train. They can also reconstruct Bayes factors with a high precision (see [8] and Section III C), which should be particularly true when compared to hierarchical inference using nested sampling, which is known to accumulate biases for example due to Monte-Carlo approximations [9, 10].

While our results show promise for this avenue of study, it is beyond the scope of this paper. However, as pointed out in [40], when Bayes factors test whether data comes from one of two mutually exclusive hypotheses, say a and $\bar{a}$, they can directly be used to calculate the posterior on the fraction of events belonging to one model over the other. They derive:

$$\log p(f_a|\vec{d}) \propto \log p(f_a) + \sum_{k=1}^{N} \log(f_a Z_k^a), + \log\left((1-f_a)Z_k^{\bar{a}}\right) \quad (5)$$

where $p(f_a|\vec{d})$ is the posterior on the fraction f_a of events coming from hypothesis a given the data $\vec{d}$, $p(f_a)$ is the prior on f_a, the index k denotes a sum over all data in $\vec{d}$, and Z_k^i is the evidence for model $i \in [a, \bar{a}]$ given data d_k. By further inserting Equation (4), we obtain:

$$\log p(f_a|\vec{d}) \propto \log p(f_a) + \sum_{k=1}^{N} -\log(1+\mathcal{B}_k) + \log(f_a + (1-f_a)\mathcal{B}_k), \quad (6)$$

where $\mathcal{B}_k$ is the Bayes factor between models a and $\bar{a}$ given data d_k. This shows that it is possible to obtain the posterior distribution by only using Bayes factors from individual events.

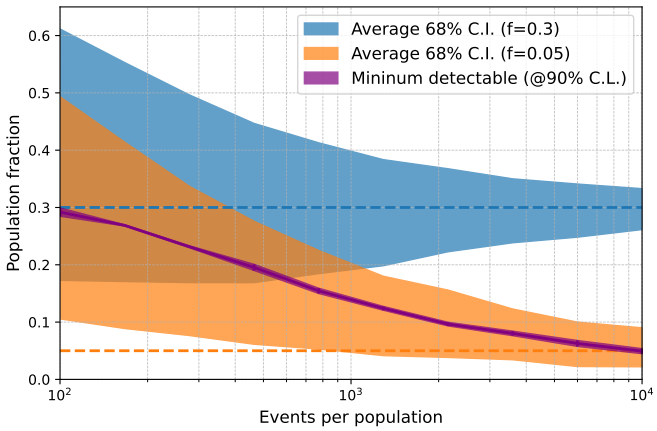


FIG. 6. *narrow purple band*: the minimum detectable true precessing fraction of events required to claim a non-zero f_a with 90% C.L, as a function of the number of events detected per population, with $1-\sigma$ uncertainty band. *blue and orange*: average reconstructed fraction, along with an uncertainty band, using Equation (6) for different injected values. The results are biased towards the positive for low number of events, because the curves are effectively cut-off at zero when the uncertainty is higher. This is reduced for higher injected values of f_a and as the number of events grows, where the distributions become Gaussian and the mean becomes unbiased. For reference, the data in this plot took about 1 min to generate.

In scenario I, the models are not technically mutually exclusive because the parameter space of aligned-spin events is a subset of the parameter space of precessing events. In practice however, the overlap between both prior spaces is negligible enough for Equation (6) to be valid. Because of how cheaply one can perform the calculation, we can easily push the calculation to 10^4 detected events per population - well beyond the numbers that the LVK is expected to measure in even the fifth observing run [41]. Even for this many events, we find that the posteriors are unbiased, meaning that the average deviations from the injected values are smaller than the average 1σ equivalent width of the posteriors. Since we can quickly obtain many posteriors for any injected fraction and number of events, it becomes trivial to also compute the fraction for which one could claim a detection. The results, which are roughly compatible with [40] where 200 Bayes Factors were calculated using nested sampling, are shown in Figure 6, where one can see that for the current number of GW detections (about 300 [7]) one would on average require a fraction of at least about 0.2 to claim a 90% C.L. measurement.

A recent population study that used data from GWTC-3[17] and large-scale galactic cluster simulations [15] finds that this fraction is below 0.15 (90% C.L.) from $10\,\mathrm{M}_\odot$ to

$40\,M_\odot$ for the primary mass, and above 0.10 from $40\,M_\odot$ to $80\,M_\odot$. This is of course not directly comparable to the numbers in this study, since data from scenario I was used in which events are drawn from a prior constructed around the posteriors measured for GW231123 [25], and only for the Hanford detector. In order to make a statement about the real binary black hole population, as opposed to our injection sets, one would also need take the detector selection function into account during data generation. These results however do demonstrate that with the methods presented in this paper it is thus possible to make fast, accurate, and most importantly scalable statements about population-scale astrophysics.

ACKNOWLEDGMENTS

The author would like to thank Sama Al-Shammari, Vivien Raymond, and Stephen Green for helpful discussions and encouragement. This work was supported by a UKRI Future Leaders Fellowship (grant number MR/Y018060/1). The author is grateful for computational resources provided by the LIGO Laboratory and supported by National Science Foundation Grants PHY-0757058 and PHY-0823459. This material is based upon work supported by NSF's LIGO Laboratory which is a major facility fully funded by the National Science Foundation.

[1] L. S. Collaboration, J. Aasi, B. Abbott, R. Abbott, T. Abbott, M. Abernathy, K. Ackley, C. Adams, T. Adams, P. Addesso, *et al.*, Advanced ligo, Classical and quantum gravity **32**, 074001 (2015).

[2] F. Acernese *et al.* (VIRGO), Advanced Virgo: a second-generation interferometric gravitational wave detector, Class. Quant. Grav. **32**, 024001 (2015), arXiv:1408.3978 [gr-qc].

[3] T. Akutsu, M. Ando, K. Arai, Y. Arai, S. Araki, A. Araya, N. Aritomi, Y. Aso, S. Bae, Y. Bae, *et al.*, Overview of kagra: Detector design and construction history, Progress of Theoretical and Experimental Physics **2021**, 05A101 (2021).

[4] A. Abac, A. Abe, I. Abouelfettouh, F. Acernese, K. Ackley, A. Adam, S. Adhicary, D. Adhikari, R. Adhikari, V. Adkins, *et al.*, Gwtc-5.0: Observations from the second part of the fourth ligo-virgo-kagra observing run and updates to the gravitational-wave transient catalog, arXiv preprint arXiv:2605.27225 (2026).

[5] G. Ashton *et al.*, BILBY: A user-friendly Bayesian inference library for gravitational-wave astronomy, Astrophys. J. Suppl. **241**, 27 (2019), arXiv:1811.02042 [astro-ph.IM].

[6] J. S. Speagle, dynesty: a dynamic nested sampling package for estimating bayesian posteriors and evidences, Monthly Notices of the Royal Astronomical Society **493**, 3132 (2020), https://academic.oup.com/mnras/article-pdf/493/3/3132/32890730/staa278.pdf.

[7] A. G. e. a. Abac, Gwtc-4.0: An introduction to version 4.0 of the gravitational-wave transient catalog, The Astrophysical Journal Letters **995**, L18 (2025).

[8] N. Jeffrey and B. D. Wandelt, Evidence networks: simple losses for fast, amortized, neural bayesian model comparison, Machine Learning: Science and Technology **5**, 015008 (2024).

[9] C. Talbot and J. Golomb, Growing pains: understanding the impact of likelihood uncertainty on hierarchical bayesian inference for gravitational-wave astronomy, Monthly Notices of the Royal Astronomical Society **526**, 3495 (2023).

[10] J. Heinzel and S. Vitale, When (not) to trust monte carlo approximations for hierarchical bayesian inference, arXiv preprint arXiv:2509.07221 (2025).

[11] T. Silva Filho, H. Song, M. Perello-Nieto, R. Santos-Rodriguez, M. Kull, and P. Flach, Classifier calibration: a survey on how to assess and improve predicted class probabilities, Machine Learning **112**, 3211 (2023).

[12] T. A. Apostolatos, C. Cutler, G. J. Sussman, and K. S. Thorne, Spin-induced orbital precession and its modulation of the gravitational waveforms from merging binaries, Phys. Rev. D **49**, 6274 (1994).

[13] R. Green, C. Hoy, S. Fairhurst, M. Hannam, F. Pannarale, and C. Thomas, Identifying when precession can be measured in gravitational waveforms, Physical Review D **103**, 124023 (2021).

[14] A. Abac, I. Abouelfettouh, F. Acernese, K. Ackley, C. Adamcewicz, S. Adhicary, D. Adhikari, N. Adhikari, R. Adhikari, V. Adkins, *et al.*, Gwtc-4.0: Population properties of merging compact binaries, arXiv preprint arXiv:2508.18083 (2025).

[15] F. Antonini, T. Callister, F. Dosopoulou, I. M. Romero-Shaw, and D. Chattopadhyay, Inferring the pair-instability mass gap from gravitational wave data, Physical Review D **112**, 063040 (2025).

[16] S. Woosley, Pulsational pair-instability supernovae, The Astrophysical Journal **836**, 244 (2017).

[17] R. Abbott, T. Abbott, F. Acernese, K. Ackley, C. Adams, N. Adhikari, R. Adhikari, V. Adya, C. Affeldt, D. Agarwal, *et al.*, Population of merging compact binaries inferred using gravitational waves through gwtc-3, Physical Review X **13**, 011048 (2023).

[18] C. Hoy, S. Fairhurst, and I. Mandel, Rarity of precession and higher-order multipoles in gravitational waves from merging binary black holes, Phys. Rev. D **111**, 023037 (2025).

[19] M. Hannam, C. Hoy, J. E. Thompson, S. Fairhurst, V. Raymond, M. Colleoni, D. Davis, H. Estellés, C.-J.

Haster, A. Helmling-Cornell, S. Husa, D. Keitel, T. J. Massinger, A. Menéndez-Vázquez, K. Mogushi, S. Ossokine, E. Payne, G. Pratten, I. Romero-Shaw, J. Sadiq, P. Schmidt, R. Tenorio, R. Udall, J. Veitch, D. Williams, A. B. Yelikar, and A. Zimmerman, General-relativistic precession in a black-hole binary, Nature **610**, 652 (2022).

[20] E. Payne, S. Hourihane, J. Golomb, R. Udall, D. Davis, and K. Chatziioannou, Curious case of gw200129: Interplay between spin-precession inference and data-quality issues, Physical Review D **106**, 104017 (2022).

[21] R. Macas, A. Lundgren, and G. Ashton, Revisiting the evidence for precession in gw200129 with machine learning noise mitigation, Physical Review D **109**, 062006 (2024).

[22] C. Hoy, R. Bondarescu, A. Lundgren, and L. K. Nuttall, A parametric signal plus noise inference framework for short duration non-gaussian noise transients, arXiv preprint arXiv:2606.31304 (2026).

[23] G. Pratten, P. Schmidt, R. Buscicchio, and L. M. Thomas, Measuring precession in asymmetric compact binaries, Physical Review Research **2**, 043096 (2020).

[24] G. Pratten, C. García-Quirós, M. Colleoni, A. Ramos-Buades, H. Estellés, M. Mateu-Lucena, R. Jaume, M. Haney, D. Keitel, J. E. Thompson, *et al.*, Computationally efficient models for the dominant and subdominant harmonic modes of precessing binary black holes, Physical Review D **103**, 104056 (2021).

[25] A. Abac, I. Abouelfettouh, F. Acernese, K. Ackley, C. Adamcewicz, S. Adhicary, D. Adhikari, N. Adhikari, R. Adhikari, V. Adkins, *et al.*, Gw231123: a binary black hole merger with total mass 190–265, The Astrophysical Journal Letters **993**, L25 (2025).

[26] V. Varma, S. E. Field, M. A. Scheel, J. Blackman, D. Gerosa, L. C. Stein, L. E. Kidder, and H. P. Pfeiffer, Surrogate models for precessing binary black hole simulations with unequal masses, Physical Review Research **1**, 033015 (2019).

[27] S. Husa, S. Khan, M. Hannam, M. Pürrer, F. Ohme, X. J. Forteza, and A. Bohé, Frequency-domain gravitational waves from nonprecessing black-hole binaries. i. new numerical waveforms and anatomy of the signal, Physical Review D **93**, 044006 (2016).

[28] S. Khan, S. Husa, M. Hannam, F. Ohme, M. Pürrer, X. J. Forteza, and A. Bohé, Frequency-domain gravitational waves from nonprecessing black-hole binaries. ii. a phenomenological model for the advanced detector era, Physical Review D **93**, 044007 (2016).

[29] `https://git.ligo.org/gwinc/pygwinc`.

[30] S. Badirli, X. Liu, Z. Xing, A. Bhowmik, K. Doan, and S. S. Keerthi, Gradient boosting neural networks: Grownet, ArXiV (2020), arXiv:2002.07971 [cs.LG].

[31] A. Paszke, S. Gross, F. Massa, A. Lerer, J. Bradbury, G. Chanan, T. Killeen, Z. Lin, N. Gimelshein, L. Antiga, *et al.*, Pytorch: An imperative style, high-performance deep learning library, Advances in neural information processing systems **32** (2019).

[32] S. Fairhurst, R. Green, C. Hoy, M. Hannam, and A. Muir, Two-harmonic approximation for gravitational waveforms from precessing binaries, Phys. Rev. D **102**, 024055 (2020).

[33] S. Fairhurst, R. Green, M. Hannam, and C. Hoy, When will we observe binary black holes precessing?, Phys. Rev. D **102**, 041302 (2020), arXiv:1908.00555 [gr-qc].

[34] A. Abac, I. Abouelfettouh, F. Acernese, K. Ackley, C. Adamcewicz, S. Adhicary, D. Adhikari, N. Adhikari, R. Adhikari, V. Adkins, *et al.*, Gw241011 and gw241110: Exploring binary formation and fundamental physics with asymmetric, high-spin black hole coalescences, The Astrophysical Journal Letters **993**, L21 (2025).

[35] I. M. Romero-Shaw, D. Gerosa, and N. Loutrel, Eccentricity or spin precession? distinguishing subdominant effects in gravitational-wave data, Monthly Notices of the Royal Astronomical Society **519**, 5352 (2023).

[36] N. Gupte, A. Ramos-Buades, A. Buonanno, J. Gair, M. Coleman Miller, M. Dax, S. R. Green, M. Pürrer, J. Wildberger, J. Macke, *et al.*, Evidence for eccentricity in the population of binary black holes observed by ligo-virgo-kagra, Physical Review D **112**, 104045 (2025).

[37] S. Tibrewal, A. Zimmerman, J. Lange, and D. Shoemaker, Misinterpreting spin precession as orbital eccentricity in gravitational-wave signals, arXiv preprint arXiv:2601.02260 (2026).

[38] J.-Q. Jiang, H.-L. Huang, J. He, Y.-T. Wang, and Y.-S. Piao, A fast deep-learning approach to probing primordial black hole populations in gravitational wave events, arXiv preprint arXiv:2505.15530 (2025).

[39] K. Leyde, S. R. Green, M. Dax, M. Mould, C. M. Fabbri, and J. Gair, End-to-end population inference from gravitational-wave strain using transformers, arXiv preprint arXiv:2605.11274 (2026).

[40] S. Vitale, R. Lynch, R. Sturani, and P. Graff, Use of gravitational waves to probe the formation channels of compact binaries, Classical and Quantum Gravity **34**, 03LT01 (2017).

[41] `https://rtd.igwn.org/projects/userguide/en/latest/capabilities.html`.